INTERNATIONAL JOURNAL OF OPTIMIZATION IN CIVIL ENGINEERING
Int. J. Optim. Civil Eng., 2025; 15(4):643-677

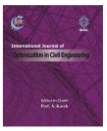

SEISMIC FRAGILITY AND RESILIENCE ASSESSMENT OF OPTIMALLY RETROFITTED RC FRAMES WITH NONLINEAR VISCOUS DAMPERS UNDER PARK–ANG DAMAGE CONSTRAINTS

M. Arjmand[1*, †], H. Naderpour[2], and A. Kheyroddin[2]
[1]*Department of Civil Engineering, Bozorgmehr University of Qaenat, Iran*
[2]*Faculty of Civil Engineering, Semnan University, Semnan, Iran*

ABSTRACT

The seismic resilience of existing reinforced concrete (RC) buildings can be improved by optimizing both energy dissipation and post-earthquake recovery. This study proposes a practical framework for upgrading RC moment-resisting frames using nonlinear fluid viscous dampers (NFVDs). Two typical frames, a four-story and an eight-story structure, were modeled and analyzed in OpenSees. Nonlinear time-history analyses with seven earthquake records were carried out to estimate the Park–Ang damage index, while incremental dynamic analyses (IDA) with 22 far-field records from FEMA P695 were used to evaluate fragility and collapse performance. The NFVDs were represented through a velocity-dependent Maxwell model, and the optimal damper parameters and locations were determined through a cost-based single-objective optimization scheme under predefined damage limits. The results show that the optimized damper configurations effectively reduced structural damage and improved post-event functionality recovery under seismic hazard levels corresponding to 10% and 2% probabilities of exceedance in 50 years. Overall, the proposed approach provides an efficient and economical solution for improving the seismic performance and resilience of existing RC frame buildings.

Keywords: Seismic resilience; Nonlinear viscous damper; Park–Ang damage index; Fragility curve; Optimization; Reinforced concrete frame.

Received: 4 November 2025; Accepted: 29 December 2025

[*]Corresponding author: *Department of Civil Engineering, Bozorgmehr University of Qaenat, Iran*
[†]E-mail address: m.arjmand@buqaen.ac.ir (M. Arjmand)

1. INTRODUCTION

RC moment-resisting frames constitute a substantial portion of the existing building stock in earthquake-prone regions. Many of these structures were originally designed according to outdated seismic provisions or gravity-load design philosophies, which has resulted in insufficient lateral strength, ductility, and energy dissipation capacity. Recent earthquakes (such as the 2023 Türkiye-Syria earthquakes) have revealed extensive structural and nonstructural damage in conventional RC buildings, highlighting the urgent need for efficient retrofit strategies that can not only prevent collapse but also ensure rapid post-earthquake functionality recovery. Within this context, seismic resilience, defined as the capacity of a structure to sustain damage and recover its function within an acceptable timeframe, has become a central concept in modern earthquake engineering. In the field of civil engineering, the effective control of structures and the mitigation of their seismic responses under earthquake excitations have consistently been among the key focuses of researchers' investigations [1,2].

Among the available retrofit strategies, energy dissipation devices have proven to be one of the most efficient means for enhancing the seismic performance of both new and existing structures. These devices reduce seismic demands by dissipating a significant portion of the input energy through inelastic or viscous mechanisms, thereby decreasing structural deformation and damage. Among various types of supplemental damping systems (such as metallic yielding dampers, viscoelastic dampers, friction dampers, and hysteretic braces) fluid viscous dampers (FVDs) have become particularly popular due to their high energy dissipation efficiency, ease of installation, and independence from external power sources [3–6].

Extensive research has demonstrated that incorporating viscous dampers into reinforced concrete (RC) or steel moment-resisting frames can significantly reduce inter-story drifts, suppress peak accelerations, and enhance energy dissipation capacity under both near-fault and far-field ground motions [7–11]. More recently, NFVDs have attracted growing attention because their velocity-dependent characteristics enable tunable damping forces that adapt to varying levels of seismic excitation. Experimental and analytical investigations have verified that nonlinear viscous behavior provides superior control of structural response at moderate and high intensity levels while preventing over-forcing at large deformations [5,7,12]. Kaveh et al. proposed a semi-active tuned mass damper (SATMD) system to mitigate vibrations in a ten-story structure subjected to four different earthquake ground motions. The SATMD configuration integrates a mass damper arranged in parallel with a magnetorheological (MR) damper, enabling adaptive control of structural response under seismic excitations [13].

Recent advances have extended viscous damping concepts to hybrid and intelligent control systems. For instance, hybrid tuned mass damper–inerter systems equipped with nonlinear viscous dampers have shown remarkable efficiency in controlling both displacement and acceleration responses of multi-story buildings [14]. Hybrid self-centering braced frames integrated with viscous dampers have been numerically shown to achieve lower floor accelerations and drifts without compromising their re-centering ability, leading to improved overall seismic performance [15]. These developments highlight the adaptability and robustness of viscous damping mechanisms in diverse structural systems.

Recent optimization frameworks have further enhanced the efficiency of viscous dampers by refining their placement and mechanical properties. Heuristic and bio-inspired algorithms (including Genetic Algorithms [16], Particle Swarm Optimization [17], and the newly developed Element Exchange Method [18]) have been successfully employed to determine optimal damper locations and damping coefficients across multiple seismic hazard levels. These methods ensure that dampers are strategically distributed where energy demands are highest, achieving substantial reductions in both peak and residual deformations while maintaining cost-effectiveness.

Overall, the cumulative evidence from recent studies confirms that properly designed nonlinear viscous dampers not only enhance the energy dissipation capacity and control damage propagation but also improve the collapse safety margin and resilience of reinforced concrete frames subjected to strong seismic events [5,7,8,17,19,20].

Traditional performance-based design approaches often rely on inter-story drift or peak displacement limits to quantify seismic performance. Although these indices adequately capture deformation demands, they fail to reflect cumulative damage and hysteretic energy dissipation that occur during earthquake loading. To overcome this limitation, damage-based indices have been developed to provide a more comprehensive assessment of structural degradation. Among them, The Park–Ang Damage Index (DI) [21] has become one of the most widely adopted measures, as it combines maximum deformation and dissipated hysteretic energy, capturing both monotonic and cyclic deterioration mechanisms. Subsequent research [12,22,23] has confirmed its robustness in correlating analytical predictions with experimental and post-earthquake observations. Nevertheless, few studies have used the Park–Ang index as an explicit design constraint in retrofit optimization problems, particularly in combination with damper systems.

A clear understanding of seismic fragility and resilience is essential when evaluating how effective a retrofit strategy can be. The two concepts describe different yet related aspects of structural performance. Fragility functions express the likelihood that a structure will exceed certain damage levels under a given ground motion intensity, while resilience indicators focus on how quickly and efficiently the structure can regain its functionality after the event. Earlier work by Cimellaro et al. [24] provided one of the first analytical frameworks linking loss estimation with functionality recovery, establishing the foundation for resilience quantification in modern earthquake engineering. Samadian et al. [25] used this concept to study existing and retrofitted RC school buildings, showing how repair cost and downtime influence the resilience index. In another contribution, Mokhtari and Naderpour [26] examined RC buildings equipped with nonlinear viscous dampers and demonstrated that properly tuned dampers can reduce both the chance of severe damage and the loss of functionality. A broader, time-dependent perspective was introduced by Ashrafifar and Estekanchi [27], who combined endurance-time analysis with corrosion modeling to evaluate how the fragility and resilience of aging bridges change over their service life. Likewise, Huang et al. [28] combined experimental testing and numerical modeling to show that friction-damped self-centering concrete frames can greatly shorten repair time and lower restoration costs compared with conventional RC frames. More recent studies have continued to refine resilience assessment frameworks: Forcellini [29] proposed a simplified yet efficient approach for quantifying resilience, and Zhao and Takahashi [30] emphasized post-earthquake functional recovery in precast and prestressed systems. Together, these investigations

highlight the importance of linking damage probability with long-term recovery capability. Despite these advances, the combined role of damage-based optimization and resilience evaluation, particularly for RC frames using nonlinear viscous dampers, has not yet been fully explored and remains a promising topic for further research.

Previous optimization studies (e.g.,[31,32]) have often adopted multi-objective formulations aimed at minimizing response quantities or maximizing energy dissipation, but they rarely provide direct control over cumulative damage. Furthermore, most of these works focus solely on fragility or dynamic response reduction, neglecting post-event resilience considerations. To address these gaps, this research proposes a single-objective, cost-based optimization framework that minimizes the total damper cost while constraining structural damage below an allowable threshold defined by the Park–Ang index. The proposed approach provides a rational basis for balancing cost efficiency, damage limitation, and seismic resilience.

In summary, this study presents a damage-constrained, cost-oriented optimization methodology for enhancing the seismic performance and resilience of RC moment-resisting frames equipped with NFVDs. Two representative buildings (a four-story and an eight-story RC frame) were analyzed under suites of far-field ground motions. The optimized damper layouts were evaluated through fragility and resilience analyses, considering both drift-based and damage-based engineering demand parameters. The main contributions of this research can be summarized as follows:

1. Development of a cost-driven, single-objective optimization model for NFVDs under explicit Park–Ang damage constraints.
2. Comparative fragility evaluation using both drift- and damage-based.
3. Integrated resilience assessment linking functionality loss, recovery rate, and resilience index.
4. Quantitative correlation between retrofit cost, damage mitigation, and resilience enhancement, offering practical guidance for engineers in resilience-oriented retrofit design.

The remainder of this paper is organized as follows. Section 2 outlines the research significance and motivation. Section 3 presents the analytical framework, including the structural models, ground motion selection and scaling, damage index formulation, nonlinear viscous damper modeling, optimization framework, and the seismic analysis, fragility, and resilience evaluation procedures. Section 4 discusses the numerical results, including optimization outcomes, damage and fragility assessments, and seismic resilience evaluations for both the four- and eight-story RC frames, followed by a comparative discussion. Finally, Section 5 summarizes the key findings and highlights the main design implications.

2. RESEARCH SIGNIFICANCE

This study advances performance-based and resilience-based design methodologies for RC structures by introducing a cost-driven, damage-controlled optimization framework. Unlike conventional multi-objective optimization approaches, which typically balance several competing criteria, the present work focuses on a single-objective minimization of damper cost while enforcing explicit Park–Ang damage constraints to ensure life-safety performance.

This formulation establishes a clear quantitative link between the economic efficiency of retrofit interventions and the physical integrity of the structure, thereby bridging the gap between engineering design objectives and resilience-oriented outcomes.
By integrating the Park–Ang damage index directly into the optimization process, the framework prevents excessive cyclic deterioration while maintaining the target performance level across all stories. In this way, the resulting retrofit design becomes not only cost-optimal but also damage-consistent along the height of the structure. Furthermore, the evaluation of the optimized configurations through both fragility analysis and resilience quantification provides a unified approach that captures immediate damage reduction as well as long-term functionality recovery. This dual evaluation perspective strengthens the reliability of the proposed method and demonstrates its suitability for real engineering applications.

From a practical standpoint, the proposed framework offers actionable guidance on determining the optimal number, placement, and parameter tuning of nonlinear viscous dampers in RC frames with varying heights. The results reveal that notable improvements in resilience can be achieved with only a modest increase in retrofit cost when realistic damage limits are imposed. Therefore, the developed approach can serve as a valuable decision-making tool for structural engineers and stakeholders who seek cost-effective yet resilient retrofit solutions for existing RC buildings in earthquake-prone regions.

3. METHODOLOGY

3.1. Overview of the Analytical Framework

The proposed methodology integrates cost-based optimization with damage-constrained design to enhance the seismic performance and resilience of RC moment-resisting frames equipped with NFVDs. The analytical framework is composed of four main stages:

(1) Numerical Modeling of RC Frames: Development of 4 and 8-story nonlinear RC MRFs (IMK model, P–Δ effects).
(2) Optimization Framework: Minimization of total damper cost under Park–Ang damage constraint ($DI\_story \leq 0.4$) .
(3) Nonlinear Time-History Analyses: Evaluation of drift and damage indices under far-field ground motions.
(4) Probabilistic Performance Evaluation: IDA, fragility (drift & DI-based), and resilience assessment leading to optimal retrofit strategies.

This workflow provides a systematic approach for linking damper optimization to damage mitigation and resilience enhancement. Figure 1 schematically illustrates the proposed process, showing how each stage contributes to the final resilience-oriented design of the structure.

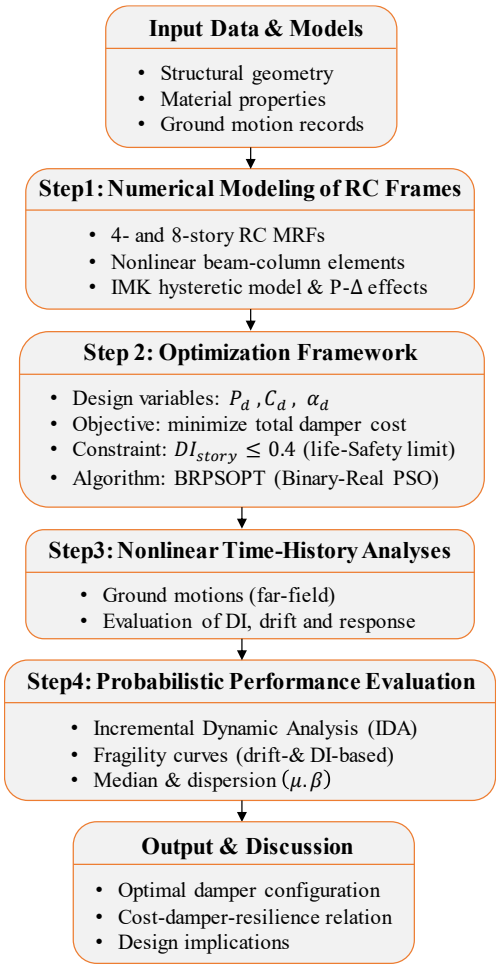

Figure 1: Schematic workflow of the proposed methodology combining damage-constrained single-objective optimization with fragility and resilience assessment of RC frames equipped with nonlinear viscous dampers.

3.2. Structural Models

Two benchmark RC moment-resisting frames (a four-story and an eight-story configuration) were analyzed to represent typical mid-rise and mid–high-rise office buildings. Both models were designed in accordance with ACI 318-02 [33], ASCE 7-02[34], and IBC 2003 provisions[35], assuming standard office loading conditions. The eight-story frame corresponds to the validated benchmark model developed by Deierlein and Haselton [36], which has also been verified by the authors in previous work [19]. The four-story frame was newly designed using consistent geometric and material properties to enable direct comparison of retrofit efficiency between the two building heights.

Concrete compressive strength and steel yield stress were assumed to be 34.5 MPa and 415 MPa, respectively. Beams and columns were modeled using elastic beam-column elements with zero-length rotational springs at both ends to capture plastic hinge formation. The cyclic deterioration of members was simulated using the modified Ibarra–Medina–Krawinkler (IMK) hysteretic model [37,38] , which accurately reproduces stiffness and strength

degradation under cyclic loading. Second-order P–Δ effects were included through geometric nonlinearity.

Figure 2 presents the geometric configurations of the analyzed frames. The four-story model was developed specifically for this study, while the eight-story frame was adopted directly from the validated benchmark database [19]. Both frames share identical material models and boundary conditions to ensure a fair comparison between controlled (retrofitted) and uncontrolled cases.

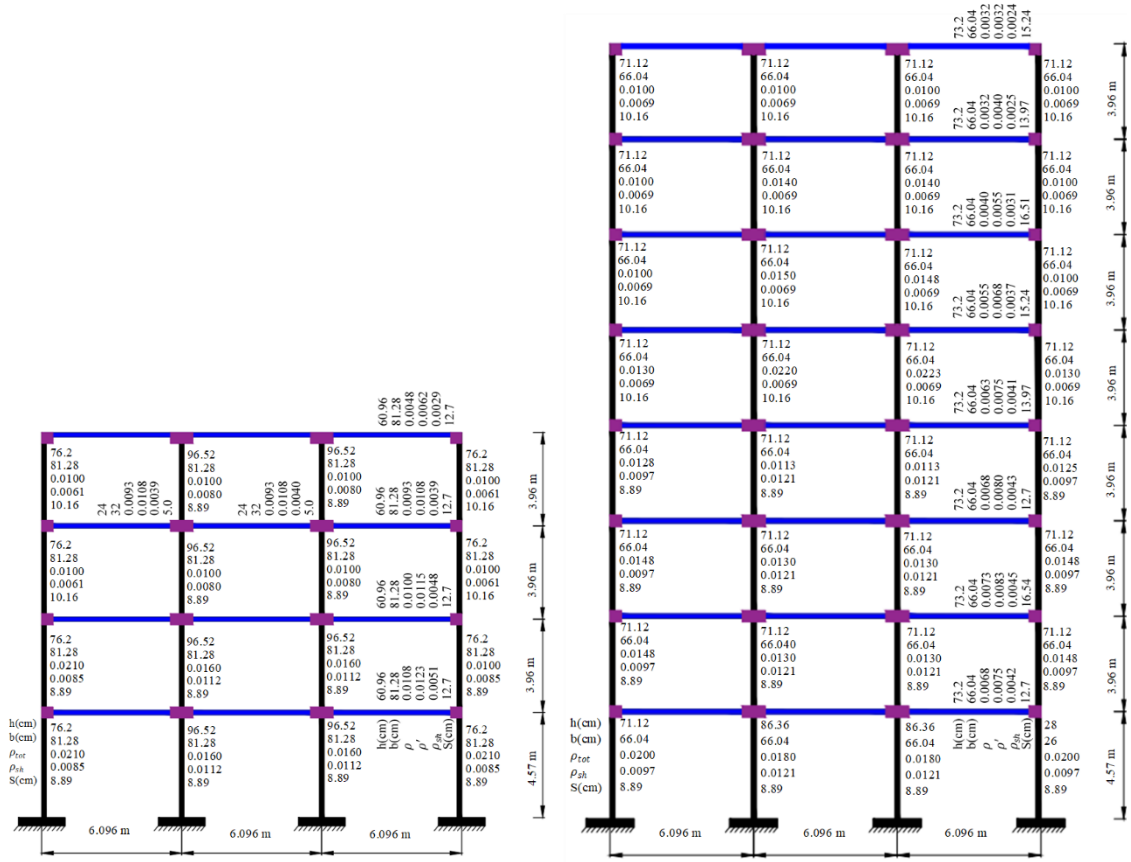

Figure 2: Geometry and dimensions of the analyzed RC moment-resisting frames: (a) the newly developed 4-story RC frame designed using consistent material and loading assumptions; (b) the 8-story benchmark frame adopted from the authors' previous study.

3.3. Ground Motion Selection and Scaling

To evaluate the seismic performance of both the four-story and eight-story RC frames, a suite of recorded far-field ground motions was selected for nonlinear dynamic analyses. Focusing on far-field records ensured consistent evaluation of overall structural behavior without the pulse-dominated effects typically associated with near-fault motions. The selected motions correspond to a high-seismicity region, represented by the site conditions of Los Angeles, California, with design spectral accelerations of $SD_s = 1.5g$ and $SD_1 = 0.9g$.

According to NEHRP classification, the site corresponds to Soil Class C, characterized by an average shear-wave velocity $V_{s-30} = 285\,m/s$. These parameters define the target design spectrum used for record scaling. A total of seven far-field earthquake records were selected based on magnitude, distance, and soil compatibility to provide adequate coverage of frequency content and intensity measures relevant to both structures. Table 1 summarizes the main characteristics of the selected motions, including the earthquake name, recording station, magnitude, and peak ground acceleration (PGA). Each record was individually scaled to match the Design Basis Earthquake (DBE) level within the fundamental period range of both frames, ensuring consistent energy input during optimization. The scaled records were used to perform nonlinear time-history analyses and to compute the Park–Ang damage indices (DI) required for the optimization stage.

Table 1: Selected far-field ground motion records used for nonlinear dynamic analyses

No	Earthquake name	Year	Station name	Magnitude	PGA (g)	PGV (cm/s)
1	Duzce Turkey	1999	Bolu	7.1	0.82	62
2	Imperial Valley-06	1979	El Centro Array #11	6.5	0.38	42
3	Kocaeli Turkey	1999	Duzce	7.5	0.36	59
4	Loma Prieta	1989	Gilroy Array #3	6.9	0.56	45
5	Northridge-01	1994	Beverly Hills - Mulhol	6.7	0.52	63
6	Imperial Valley-06	1979	Delta	6.5	0.35	33
7	Superstition Hills-02	1987	El Centro Imp. Co. Cent	6.5	0.36	46

Figure 3 compares the target design spectrum with the scaled response spectra of the selected ground motions. As shown, the spectra exhibit close agreement in the period range of interest, validating the use of a single ground motion suite for both frames.

3.4. Damage Index and Energy Dissipation Evaluation

To quantify the structural damage of the RC frames under seismic loading, the Park–Ang damage index [21] was adopted. This index accounts for both maximum deformation and cumulative hysteretic energy, providing a comprehensive measure of deterioration caused by repeated inelastic cycles. The general form of the index is expressed as:

$$DI_{PA} = \frac{\delta_m}{\delta_u} + \frac{E_h}{\delta_u F_y}\beta \tag{1}$$

where δ_m and δ_u are the maximum and ultimate deformations, respectively; E_h denotes the cumulative hysteretic energy dissipated by the member, F_y is the yielding force, and β is a model parameter that represents the effect of cyclic degradation. This hybrid formulation combines deformation demand and energy dissipation, offering a more realistic representation of cumulative damage than deformation-based measures alone. A detailed description of the modified Park–Ang index and its implementation at the frame level can be found in Arjmand et al. [19]. The hysteretic energy E_h of each element was obtained from nonlinear time-

history analyses by integrating the product of internal forces and corresponding deformations over the entire earthquake duration, as expressed by:

$$E_h = \int (Nd\Delta + Md\theta + Vd\gamma) \tag{2}$$

where N, M, and V represent the axial force, bending moment, and shear force, while $d\Delta$, $d\theta$, and $d\gamma$ are the corresponding incremental deformations. The total hysteretic energy for each story and for the entire structure was computed by summing the contributions of individual members. This provided the basis for evaluating both global damage and energy dissipation efficiency, which are essential for assessing the effectiveness of the retrofitted configurations.

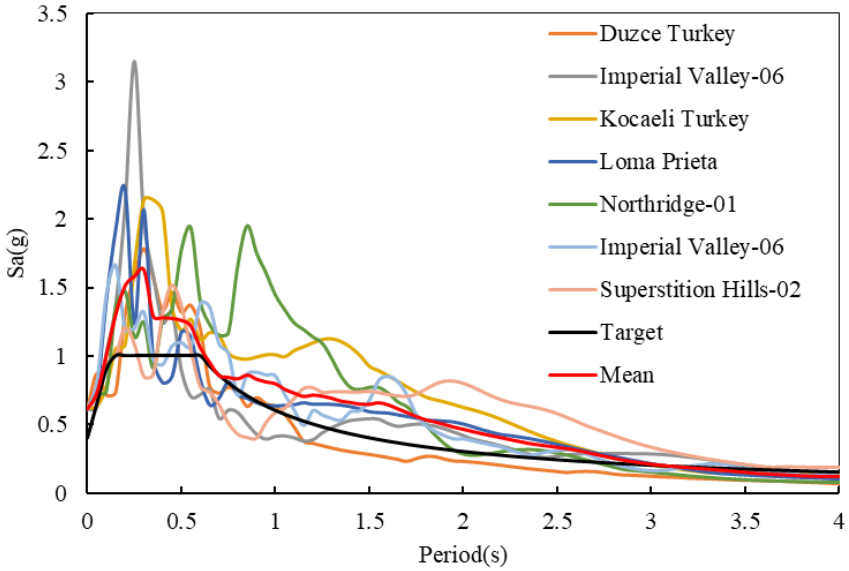

Figure 3: Target design spectrum and scaled response spectra of the selected far-field ground motions used for both the 4-story and 8-story RC moment-resisting frames.

3.5. Modeling of Nonlinear Viscous Dampers

The NFVDs were modeled in OpenSees [39] using the twoNodeLink element combined with the ViscousDamper material. The nonlinear force–velocity relationship governing the damper behavior is expressed as:

$$F_d = c_d \left|\dot{u}_d\right|^{\alpha} \operatorname{sgn}(\dot{u}_d) \tag{3}$$

where c_d and α denote the damping coefficient and velocity exponent, respectively. This relationship allows the device to develop velocity-dependent resisting forces that dissipate seismic input energy without significantly altering the global stiffness of the structure. To capture the frequency-dependent stiffness of the entire damper assembly

(including the brace, gusset plate, and clevis bracket) the Maxwell model was employed. The equivalent stiffness of the system can be represented as:

$$\frac{1}{K_s} = \frac{1}{K_d} + \frac{1}{K_b} + \frac{2}{K_{cl}} + \frac{2}{K_{gus}} \tag{4}$$

where K_s, K_d, K_b, K_{gus}, K_{cl} correspond to the equivalent stiffness of the overall system, the viscous device, the brace, the gusset plate, and the clevis bracket, respectively. This formulation ensures that both the viscous behavior and mechanical flexibility of the damper components are accurately captured, reflecting the actual performance of commercial damper assemblies. Additional details regarding the mechanical representation and parameter calibration can be found in Arjmand et al. [19].

3.6. Optimization Framework

The optimization process in this study aims to determine the most efficient configuration of NFVDs that minimizes the total retrofit cost while maintaining the desired damage performance level. The cost function adopted here is based on the empirical relationship proposed by Gidaris and Taflanidis [40], which correlates the initial cost of commercial fluid viscous dampers to their maximum design force. According to their regression analysis of market data, the total cost of a damper can be estimated as a power-law function of its maximum design force F_{MAX} (in kN):

$$\mathrm{Cos}\,t_{damper} = \$96.88(F_{MAX,j})^{0.607} \tag{5}$$

This equation reflects the manufacturing and installation costs of fluid viscous dampers, where the coefficient (96.88) and the exponent (0.607) were derived from regression analysis of price data provided by manufacturers such as Taylor Devices. Accordingly, the objective function of the optimization problem is expressed as the minimization of the total damper cost:

Find : $$X = \{P, C_{d}$$

Minimize: $$f(X) = \min(\frac{1}{N_{eq}} \sum_{j=1}^{Nd} 96.88 \tag{6}$$

subject to the following constraints:

$$C_{d,\min}$$

$$\alpha_{d,\min} :$$

where $X = \{P, C_d, \alpha_d\}$ denotes the vector of design variables, including the damper placement, damping coefficients, and velocity exponents. $F_{MAX,j}$ is the peak damper force obtained from nonlinear time-history analyses under the DBE level and $g_j(X)$ represents behavioral constraints ensuring that the Park–Ang damage index remains within allowable limits for all stories.

The optimization problem was solved using the Particle Swarm Optimization (PSO) algorithm, chosen for its robustness and fast convergence in nonlinear and nonconvex search spaces. The external penalty function method was applied to handle inequality constraints effectively. In the PSO framework, each "particle" represents a potential damper configuration, and its position and velocity are iteratively updated based on its own best experience and the swarm's global best solution. This approach allows the search to balance exploration and exploitation, leading to efficient identification of the optimal configuration that minimizes retrofit cost while ensuring uniform damage distribution and satisfactory seismic performance. The optimized damper layouts obtained from this process form the basis for the subsequent fragility and resilience assessments presented in Section 4.

3.7. Seismic Analysis, Fragility, and Resilience Evaluation

A comprehensive seismic performance assessment was carried out to evaluate the fragility and resilience of the studied RC MRFs, both with and without NFVDs. The procedure consisted of four main phases: (i) nonlinear dynamic analysis, (ii) derivation of fragility functions, (iii) resilience quantification, and (iv) modeling of post-earthquake recovery.

(a) Nonlinear Dynamic Analysis

The structural models were developed in OpenSees, incorporating both material and geometric nonlinearities to simulate realistic inelastic response. Each model was subjected to suites of far-field ground motions, selected and scaled according to the recommendations of FEMA P695 [41] to match the site-specific design spectrum. The Incremental Dynamic Analysis (IDA) approach [42] was adopted using the Hunt–Fill algorithm, which adaptively refines intensity steps near collapse to improve numerical accuracy compared with the conventional constant-step method. For each ground motion record, the spectral acceleration at the first-mode period Sa(T1) was selected as the intensity measure (IM), while the maximum interstory drift ratio (IDR) served as the damage measure (DM). The resulting IDA curves describe the structural response under increasing ground motion intensity and enable the identification of key limit states (Immediate Occupancy (IO), Life Safety (LS), and Collapse Prevention (CP)) as defined in FEMA P695[41].

(b) Fragility Function Development

Seismic fragility functions were derived from the IDA results to quantify the conditional probability of exceeding specific damage states under various seismic intensities. Four discrete damage states (Slight, Moderate, Extensive, and Complete) were defined following the HAZUS-MH guidelines [43]. For each damage state, the median spectral acceleration $S_{a,50}$ (corresponding to 50% probability of exceedance) and the logarithmic standard

deviation β were determined, assuming a lognormal distribution of structural response. The fragility function can be expressed as:

$$F = P(D \geq C \mid IM) = 1 - \Phi\left(\frac{LnC - m_x(IM)}{\sigma_x}\right) \tag{7}$$

where $P(D \geq C \mid IM)$ denotes the probability of exceeding the C-th damage limit state for a given intensity measure IM , $m_x(IM)$ is the median demand, σ_x denotes the standard deviation of the natural logarithm of response and Φ is the standard normal cumulative distribution function. At the extreme limit, the maximum interstory drift ratio (IDR) associated with each structural damage level (Slight, Moderate, Extensive, and Complete) was taken from the threshold values recommended by HAZUS, summarized in Table 2. A rightward shift in the fragility curve indicates increased seismic capacity and reduced vulnerability, consistent with recent advances in performance-based earthquake engineering [19,31,44].

Table 2: Structural level of damage for an Office building based on HAZUS [45]

Office building type	Description	Inter-story drift ratio at level of damage			
		Slight	Moderate	extensive	complete
C1H	High-rise concrete moment frame building	0.0025	0.0050	0.0150	0.0400
C1L	Mid-rise concrete moment frame building	0.0033	0.0067	0.0200	0.0533

(c) Seismic Resilience Framework

The seismic resilience evaluation followed the conceptual framework proposed by Cimellaro et al. [24], defining resilience as the ability of a system to withstand, absorb, and recover its functionality after a seismic event. This framework integrates damage, losses, and functionality recovery into a single performance metric, the Resilience Index (RI).

The assessment involved four major steps:

1. Developing fragility functions to estimate the probability of exceeding each damage state at different ground-motion intensities.
2. Estimating physical damage and the corresponding direct and indirect economic losses.
3. Deriving functionality loss and recovery curves, representing the temporal variation of operational capacity after an earthquake.
4. Computing the RI as the normalized area under the functionality recovery curve.

The loss of functionality was derived from the expected physical damage estimated through drift-based fragility functions, which relate the probability of exceeding specific damage states to the corresponding spectral acceleration levels. These fragility relationships were

subsequently used to determine repair costs and downtime for structural and nonstructural components within the resilience assessment framework.

The loss of functionality was derived from the expected physical damage estimated through the drift-based fragility curves, which relate the probability of exceeding certain damage states to the corresponding spectral accelerations. These relationships were used to compute repair costs and downtime for structural and nonstructural components based on the HAZUS-MH technical manual [45]. The ratios of building repair cost to replacement cost (Cs/Is) for structural, acceleration-sensitive nonstructural, and drift-sensitive nonstructural components are summarized in Table 3. These values were employed to convert component-level damage into direct and indirect losses, which form the basis for estimating overall functionality loss and recovery duration.

Table 3: Ratio of Building Repair Cost to Replacement Cost (in Percent)

Components	Cs/Is (%)			
	Slight	Moderate	Extensive	Complete
Structural components	0.4	1.9	9.6	19.2
Acceleration-sensitive non-structural components	0.9	4.8	14.4	47.9
Drift-sensitive nonstructural components	0.7	3.3	16.4	32.9

The RI was then calculated using the formulation proposed by Cimellaro et al. [24]:

$$RI = \int_{t_{OE}}^{t_{OE}+T_{RE}} \frac{Q(t)}{T_{RE}} dt \tag{8}$$

where Q(t) represents the functionality level of the structure at time t; t_{OE} is the time of the seismic event; and T_{RE} is the total recovery duration required to regain full functionality. A higher RI value indicates better robustness and faster recovery. The overall workflow of this process is illustrated in Figure 4.

(d) Recovery Modelling

Post-earthquake recovery trajectories were represented using three common functional forms, depending on resource availability and management efficiency [24]:

- Linear recovery: representing limited resources and constant restoration rate.
- Exponential recovery: corresponding to rapid reconstruction supported by efficient resource allocation.
- Trigonometric recovery: modeling an initial delay followed by accelerated restoration as coordination improves.

The selected recovery model determines the slope of the functionality curve and consequently influences the overall value of the resilience index.

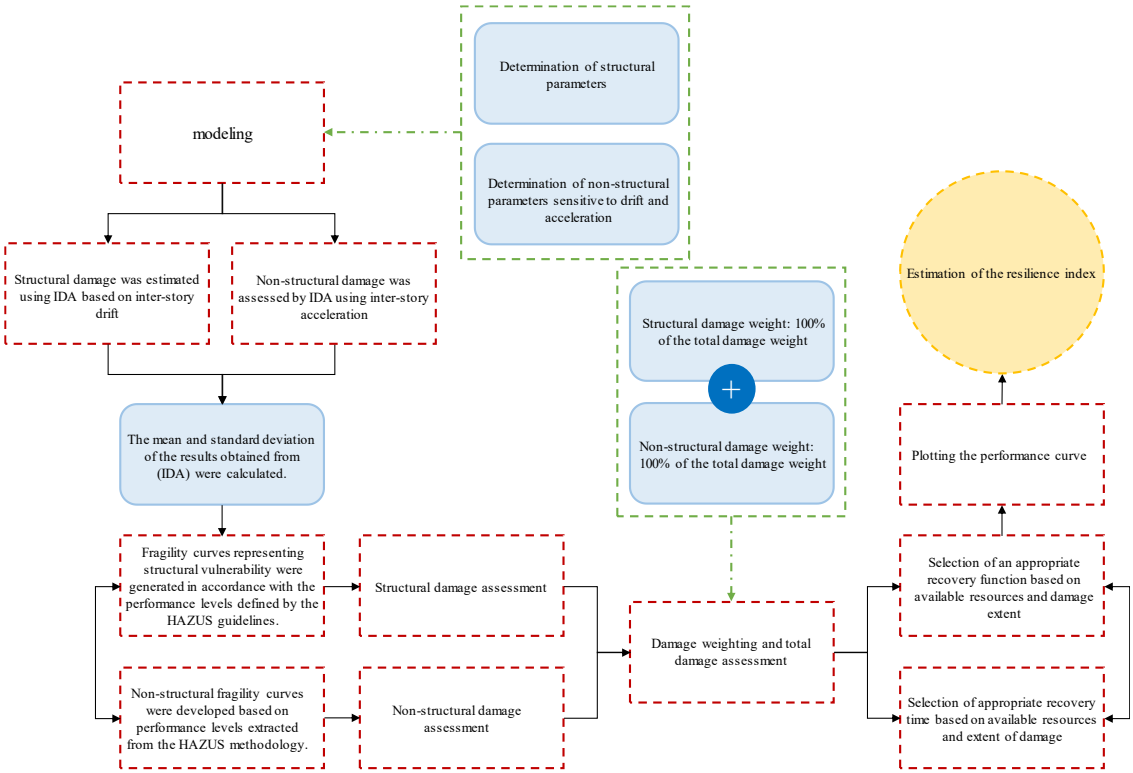

Figure 4: Flowchart of the seismic resilience assessment framework used in this study

4. RESULTS AND DISCUSSION

This section presents the outcomes of nonlinear dynamic analyses, optimization, and seismic resilience evaluation for the two RC moment-resisting frames studied. The results are organized into four main parts:

(1) an overview of the analytical program,
(2) optimization results and damper characteristics,
(3) damage and fragility analysis based on the Park–Ang damage index, and
(4) assessment of seismic resilience and functionality recovery

4.1. Overview of the Analytical Program

Two prototype RC moment-resisting frames, one with four stories and the other with eight, were analyzed to examine the efficiency of NFVDs in reducing seismic damage and enhancing structural resilience. All modeling assumptions, material properties, and loading conditions were kept consistent between the two structures so that any differences in performance could be attributed solely to structural height and the inclusion of optimized dampers. For each frame, two configurations were evaluated: (i) the uncontrolled frame, representing the original structure without dampers, and (ii) the controlled frame, retrofitted with optimally configured NFVDs. Both models shared identical geometry, reinforcement detailing, and boundary

conditions, allowing direct comparison of their dynamic and damage responses. The analytical program followed a systematic sequence comprising five key stages:

1. Performing nonlinear time-history analyses under multiple seismic hazard levels to capture global and local structural responses.
2. Conducting single-objective optimization to identify the optimal number, placement, and mechanical parameters of the dampers, minimizing retrofit cost while satisfying the damage constraint.
3. Calculating the Park–Ang damage index (DI) to quantify local and global damage under each analysis case.
4. Developing fragility curves based on the probability of exceeding defined damage states using both drift-based and damage-based parameters.
5. Evaluating seismic resilience using a loss–recovery approach that estimates post-earthquake functionality and computes the resilience index.

It should be noted that in the authors' previous work [19], fragility analyses for the eight-story frame were conducted only on the basis of interstory drift ratios. In the present study, new Park–Ang–based fragility curves are introduced for the same structure to provide a more comprehensive evaluation of seismic performance. These analyses provided the foundation for evaluating the optimization results, fragility behavior, and resilience performance of the studied RC frames, which are discussed in the following sections.

4.2. Optimization Results and Damper Characteristics

The optimization process aimed to minimize the total retrofit cost while maintaining the target performance level defined by the Park–Ang damage constraint. The hybrid Binary–Real Particle Swarm Optimization with Passive Congregation (BRPSOPC) algorithm was employed for this purpose, demonstrating fast convergence and strong stability for nonlinear, multi-parameter problems. For each structural model, several retrofit scenarios were investigated to examine the influence of the number of dampers on cost efficiency and energy dissipation. Specifically, configurations with one, three, and four dampers were analyzed for the four-story frame, while the eight-story frame was optimized for layouts containing four, six, and eight dampers. The algorithm successfully identified optimal damper locations and mechanical parameters, yielding stable solutions in fewer than 200 iterations. In all cases, the optimization balanced two competing objectives: maximizing energy dissipation capacity and minimizing the total damper cost.

4.2.1. Four-story Frame

The optimization results for the four-story frame are summarized in Table 4, which lists the optimal damper locations, mechanical parameters, and objective costs for three retrofit configurations. In the single-damper case, the optimal placement occurred at the second story, corresponding to the floor with the highest interstory energy demand.

Table 4: Optimal damper locations, mechanical parameters, and objective costs for the 4-story frame.

Story	1 Damper		3 Dampers		4 Dampers	
	$C_d\,(kN.\text{sec}/\,mm)$	α_d	$C_d\,(kN.\text{sec}/\,mm)$	α_d	$C_d\,(kN.\text{sec}/\,mm)$	α_d
1	–	–	1.85	0.106	34.96	0.306
2	32.16	0.81	34.93	0.582	1.75	0.10
3	–	–	–	–	1.75	0.102
4	–	–	1.75	0.110	1.75	0.10
Objective cost ($)	15141.64		14983.36		12911.15	

Note: "–" indicates that no damper was assigned to that story.

For the three-damper configuration, dampers were positioned at the first, second, and fourth stories, creating a more balanced energy dissipation profile. Finally, in the four-damper configuration, one damper was installed on each story, achieving the most uniform energy distribution and the lowest objective cost ($12911.15).

The optimized parameters indicate a gradual shift from nearly linear to strongly nonlinear viscous behavior as the number of dampers increases. Overall, increasing the number of dampers improved both energy dissipation uniformity and economic efficiency. The optimal locations were consistently concentrated in the lower and middle stories, where seismic energy demand was most significant.

4.2.2. Eight-story Frame

Optimization results for the eight-story frame are summarized in Table 5, which presents the optimal damper placements, mechanical parameters (C_d and α_d), and the corresponding objective costs for retrofit cases involving four, six, and eight dampers.

For the four-damper configuration, the algorithm concentrated the devices primarily in the second, fifth, and eighth stories, where the highest interstory energy demands were recorded. This layout resulted in moderately nonlinear behavior and an objective cost of $17749.76.

When the number of dampers increased to six, the devices were distributed from the first to seventh stories, providing a smoother energy dissipation pattern along the height of the structure. The corresponding damping coefficients ranged from C_d =16.30 to 25.93 $kN.\text{sec}/\,mm$, with velocity exponents α_d =0.32–0.93, indicating an effective level of nonlinearity. This configuration achieved the lowest total cost ($14650.65), demonstrating an optimal balance between performance and economy.

For the eight-damper configuration, dampers were assigned to all stories, resulting in the most uniform response but a slightly higher cost ($17544.64) due to the larger number of devices required.

Overall, the six-damper configuration was identified as the most efficient design, achieving cost-effective and uniform energy dissipation without redundancy. In all optimized cases, dampers were concentrated mainly between the second and fifth stories, aligning with regions of maximum energy and damage demand. These observations are consistent with findings by Mohemmi et al. [7] and Sebaq et al. [12], who reported similar optimal damper locations and parameter ranges for multi-story RC and steel frames.

Table 5: Optimal damper locations, mechanical parameters, and objective costs for the 8-story frame.

Story	4 Dampers		6 Dampers		8 Dampers	
	$C_d\,(kN.\text{sec}/\,mm)$	α_d	$C_d\,(kN.\text{sec}/\,mm)$	α_d	$C_d\,(kN.\text{sec}/\,mm)$	α_d
1	–	–	23.58	0.93	34.86	0.256
2	34.96	0.54	16.30	0.34	2.71	0.127
3	1.76	0.17	19.79	0.32	1.75	0.10
4	–	–	25.93	0.46	1.79	0.10
5	12.74	0.29	–	–	1.75	0.10
6	–	–	17.91	0.48	1.77	0.49
7	–	–	–	–	1.77	0.15
8	1.75	0.87	24.62	0.597	1.87	0.43
Objective cost ($)	17749.76		14650.65		17544.64	

Note: "–" indicates that no damper was assigned to that story.

4.3. Damage Evaluation and Fragility Analysis

This section examines the extent of structural damage and evaluates the seismic vulnerability of the studied RC frames through both drift-based and Park–Ang–based fragility analyses. The results provide insight into how the optimized nonlinear viscous dampers influence the distribution and severity of damage under various ground motion intensities.

4.3.1. Four-Story Frame – Damage Evaluation Based on the Park–Ang Damage Index

The overall and story-level Park–Ang damage indices for the four-story RC frame, with and without nonlinear viscous dampers, are summarized in Tables 6 and 7. The inclusion of optimized dampers led to a notable reduction in both global and local damage indices across all earthquake records. The mean global DI of the uncontrolled frame was 0.593, which decreased to 0.399, 0.395, and 0.349 for the configurations with one, three, and four dampers, respectively; representing reductions of about 33–41% compared with the unretrofitted case.

Table 6: Global Park–Ang damage index values for the 4-story frame

Earthquake	w/o FVD	With FVD		
		w/1 FVD	w/3 FVD	w/4 FVD
Duzce Turkey	0.245	0.141	0.133	0.115
Imperial Valley-06	0.380	0.152	0.143	0.139
Kocaeli Turkey	0.614	0.583	0.602	0.544
Loma Prieta	0.710	0.345	0.325	0.290
Northridge-01	0.650	0.439	0.584	0.447
Imperial Valley-06	0.772	0.515	0.470	0.475
Superstition Hills-02	0.783	0.622	0.510	0.433
Mean	0.593	0.399(32.7[a])	0.395(33.4)	0.349(41.1)

[a] Reduction percentage with FVD compared to without FVD

According to the Park–Ang criterion, this shift indicates that the addition of dampers effectively transformed the global damage state from irreparable to repairable. At the story level (Table 7), the maximum DI dropped from 0.637 in the uncontrolled frame to around

0.400 for all controlled configurations, corresponding to an average reduction of approximately 37%. The variance of story-wise DI values also declined by nearly 84%, suggesting that the damage distribution became considerably more uniform along the height of the structure.

Table 7: Story-level Park–Ang damage indices.

		With FVD		
Story level	w/o FVD	w/1 FVD	w/3 FVD	w/4 FVD
1	0.637	0.400	0.353	0.400
2	0.466	0.259	0.400	0.319
3	0.216	0.132	0.364	0.178
4	0.040	0.196	0.082	0.210
Maximum	0.637	0.400(37.20[a])	0.400(37.20)	0.400(37.20)
Mean	0.340	0.247(37.65)	0.300(11.76)	0.277(18.53)
Variance	0.052	0.010(80.77)	0.016(69.23)	0.008(84.61)
g_1 value	0.597	0.268(55.11)	0.318(46.73)	0.222(62.81)

[a] Reduction percentage with FVD compared to without FVD.

Figure 5 illustrates the average story-wise DI profiles for the uncontrolled and controlled cases. As shown, the presence of viscous dampers clearly smoothed the damage distribution, particularly in the lower and middle stories where nonlinear deformations were most pronounced in the bare frame. This uniformity reflects the ability of the optimized NFVDs to dissipate seismic energy efficiently and to prevent the concentration of plastic demands in specific stories.

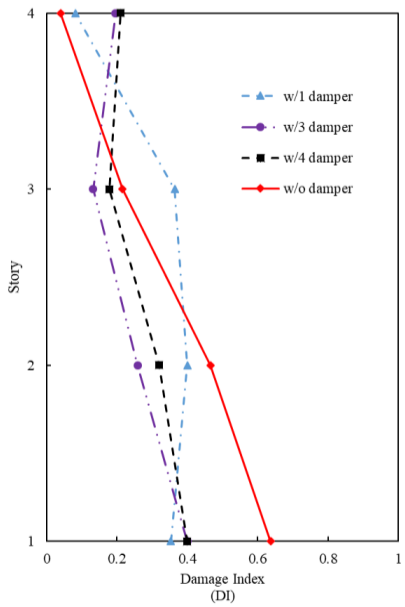

Figure 5: Average story damage index distribution for controlled and uncontrolled configurations.

4.3.2. Four-Story Frame - Fragility Analysis (Drift-based and Park-Ang-based)

The seismic fragility of the four-story frame was evaluated using two distinct engineering demand parameters (EDPs): the interstory drift ratio (IDR) and the Park–Ang damage index. This dual-parameter approach allows assessment of the structure from both deformation and cumulative-damage perspectives.

(a) Drift-based Fragility

Drift-based fragility curves for the four defined damage states (Slight, Moderate, Extensive, and Complete) were developed using the IDA results for 22 far-field ground motions specified in FEMA P695. As illustrated in Figure 6, the fragility curves for the damped configurations exhibit a consistent rightward shift relative to the uncontrolled frame, indicating a reduced probability of exceeding any given damage state at the same spectral acceleration level.

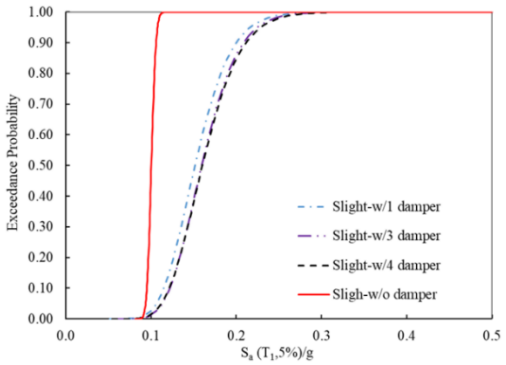

(a) Slight damage

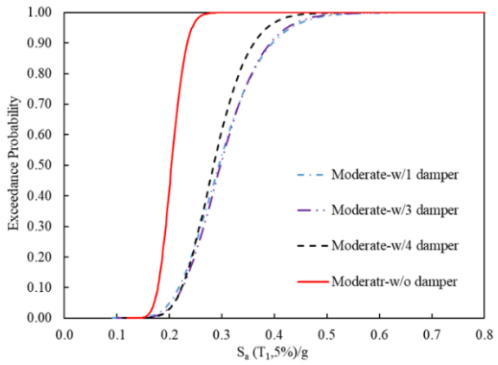

(b) Moderate damage

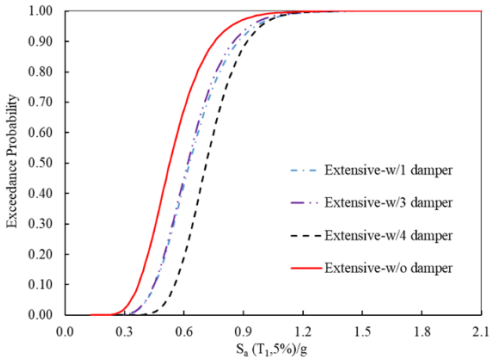

(c) Extensive damage

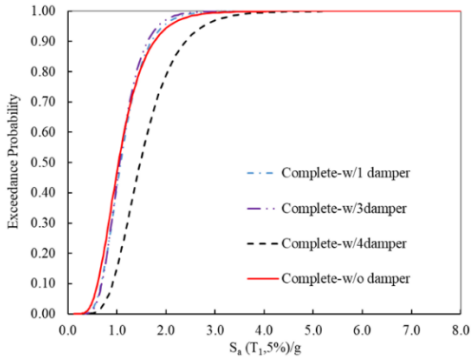

(d) Complete damage

Figure 6: Drift-based fragility curves for the 4-story RC frame corresponding to slight, moderate, extensive, and complete damage states

Table 8 lists the median spectral accelerations corresponding to 50% probability of exceedance for each damage state. For the four-damper configuration, the median Sa increased by approximately 60%, 40%, 34%, and 45% at the Slight, Moderate, Extensive, and Complete damage levels, respectively, compared with the bare frame.

Table 8: Median spectral acceleration and improvement percentages for each damage state based on inter-story drift for the 4-story RC frame

Condition	Sa corresponding to the mean P_f			
	Slight	Moderate	Extensive	Complete
w/o damper	0.10	0.20	0.52	1.03
w/1 damper	0.15(50.0[a])	0.29(45.0)	0.62(19.23)	1.07(3.88)
w/3 damper	0.16(60.0)	0.30(50.0)	0.61(17.31)	1.05(1.94)
w/4 damper	0.16(60.0)	0.28(40.0)	0.70(34.61)	1.49(44.66)

[a] Reduction percentage with FVD compared to without FVD.

These increases confirm that optimized viscous damping substantially enhances lateral strength and reduces overall seismic vulnerability.

The differences in failure probability between controlled and uncontrolled configurations are depicted in Figure 7 The largest reductions occurred in the Slight (~95%) and Moderate (~78%) damage states, indicating that NFVDs are most effective in mitigating minor-to-moderate damage, which is crucial for preserving post-earthquake functionality.

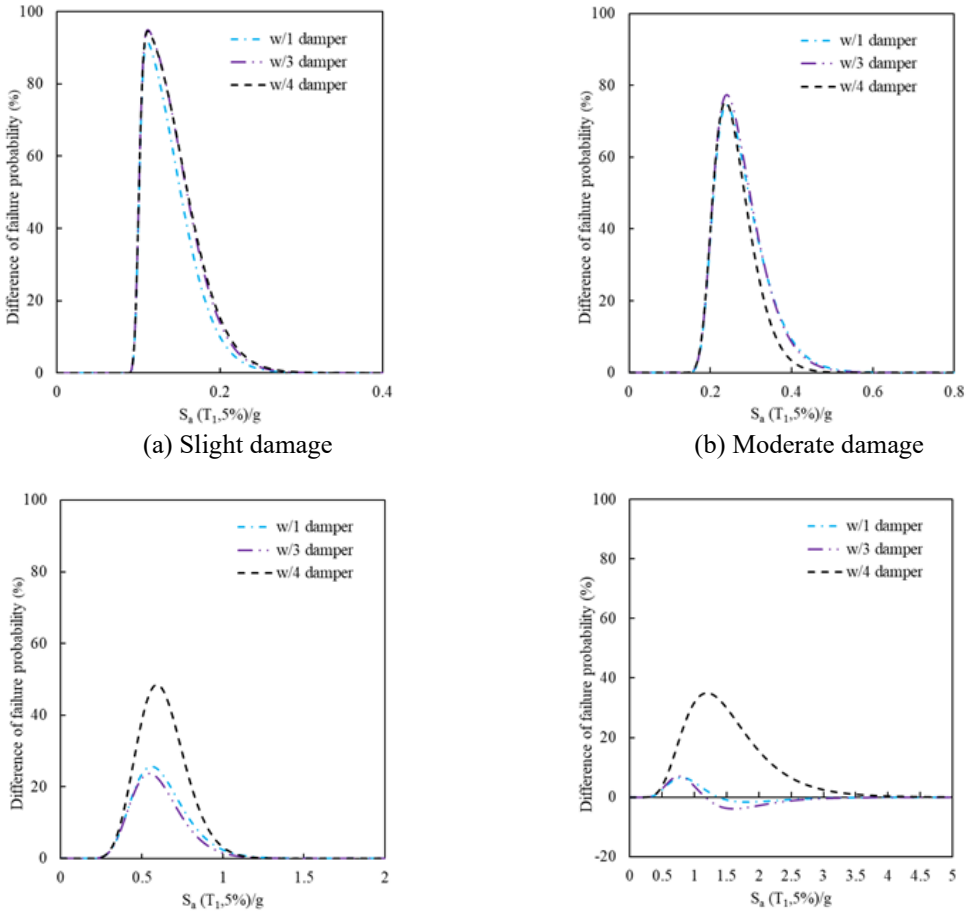

(a) Slight damage (b) Moderate damage

(c) Extensive damage (d) Complete damage

Figure 7: Difference in failure probability between uncontrolled and controlled 4-story RC frames based on inter-story drift.

(b) Park–Ang-based Fragility

Fragility curves based on the Park–Ang damage index are presented in Figure 8, offering a cumulative damage perspective that accounts for both deformation and energy dissipation. The trends are consistent with the drift-based results, but the slopes of the curves are steeper, reflecting reduced dispersion in the response once energy absorption is considered.

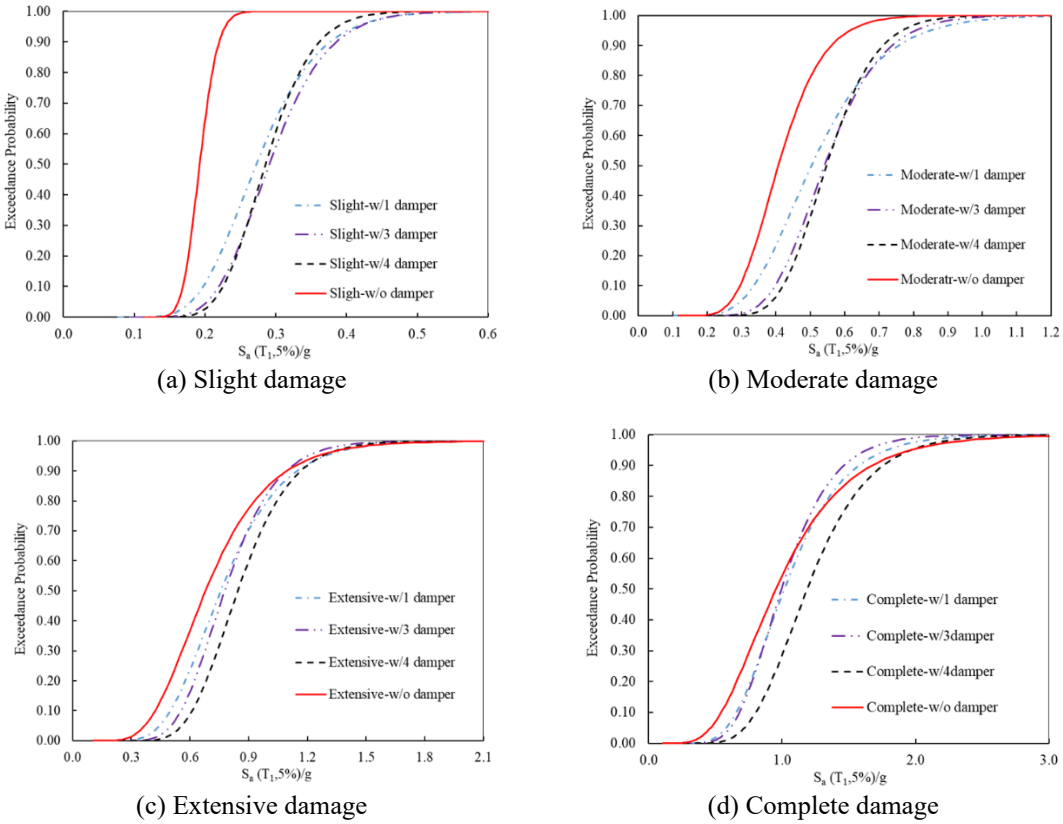

(a) Slight damage (b) Moderate damage

(c) Extensive damage (d) Complete damage

Figure 8. Drift-based fragility curves for the 4-story RC frame corresponding to slight, moderate, extensive, and complete damage states

Table 9 summarizes the median spectral accelerations obtained from the DI-based fragility analysis. For the four-damper configuration, the median Sa values increased by roughly 47%, 32%, 24%, and 25% for the Slight, Moderate, Extensive, and Complete damage states, respectively, relative to the uncontrolled structure. This confirms that including hysteretic energy effects yields a more reliable measure of seismic performance, particularly for assessing retrofit efficiency.

As shown in Figure 9, the maximum reduction in exceedance probability reached approximately 83% for the Slight state and remained significant (around 49%) even for the Complete state. These results underscore the effectiveness of optimized NFVDs in reducing both the magnitude and likelihood of damage exceedance, leading to improved reliability and robustness under strong earthquakes.

Overall, comparison between the drift-based and DI-based fragility analyses demonstrates that optimized viscous dampers not only increase the median intensity measure for each damage state but also flatten the fragility curves, indicating reduced response uncertainty and improved resilience. This dual improvement in strength and predictability confirms the superior capability of NFVDs in achieving balanced seismic performance for RC frames.

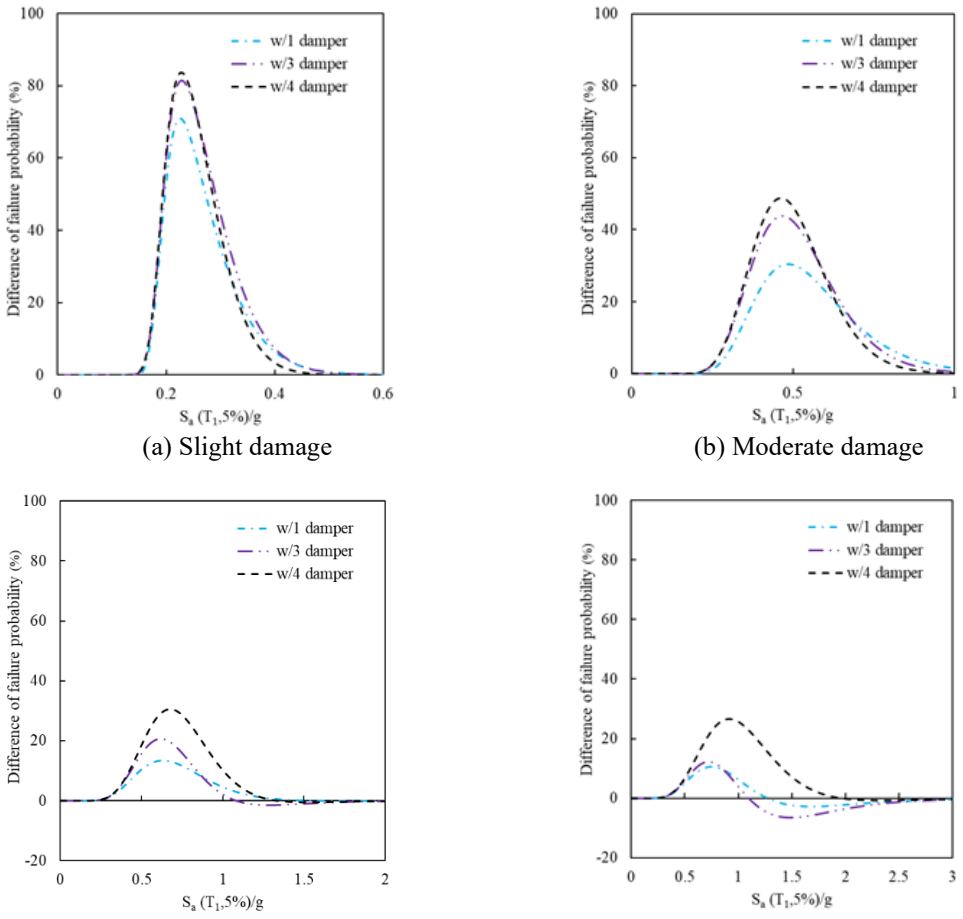

(a) Slight damage (b) Moderate damage

(c) Extensive damage (d) Complete damage

Figure 9. Difference in failure probability between uncontrolled and controlled 4-story RC frames (Park–Ang-based).

Table 9: Median spectral acceleration (Sa) and improvement percentages for each damage state based on the Park–Ang damage index

Condition	Sa corresponding to the mean P_f			
	Slight	Moderate	Extensive	Complete
w/o damper	0.19	0.41	0.68	0.95
w/1 damper	0.27(42.1[a])	0.50(21.9)	0.75(10.3)	1.02(7.4)
w/3 damper	0.29(52.6)	0.53(29.3)	0.77(13.2)	0.99(4.2)
w/4 damper	0.28(47.4)	0.54(31.7)	0.84(23.5)	1.19(25.3)

[a] **Reduction percentage with FVD compared to without FVD.**

4.3.3. Eight-Story Frame – Fragility Analysis (Park–Ang-based)

The fragility analysis for the eight-story RC frame was performed using the Park–Ang damage index as the EDP, allowing simultaneous consideration of deformation and cumulative energy dissipation. This approach provides a realistic estimation of the probability of exceeding various damage states at different ground-motion intensities.

As shown in Figure 10, all damped configurations (four-, six-, and eight-damper layouts) exhibit a noticeable rightward shift of the fragility curves compared with the uncontrolled frame, reflecting lower vulnerability and greater seismic capacity. The slopes of the fragility functions also become slightly flatter, indicating reduced dispersion and enhanced stability of structural response.

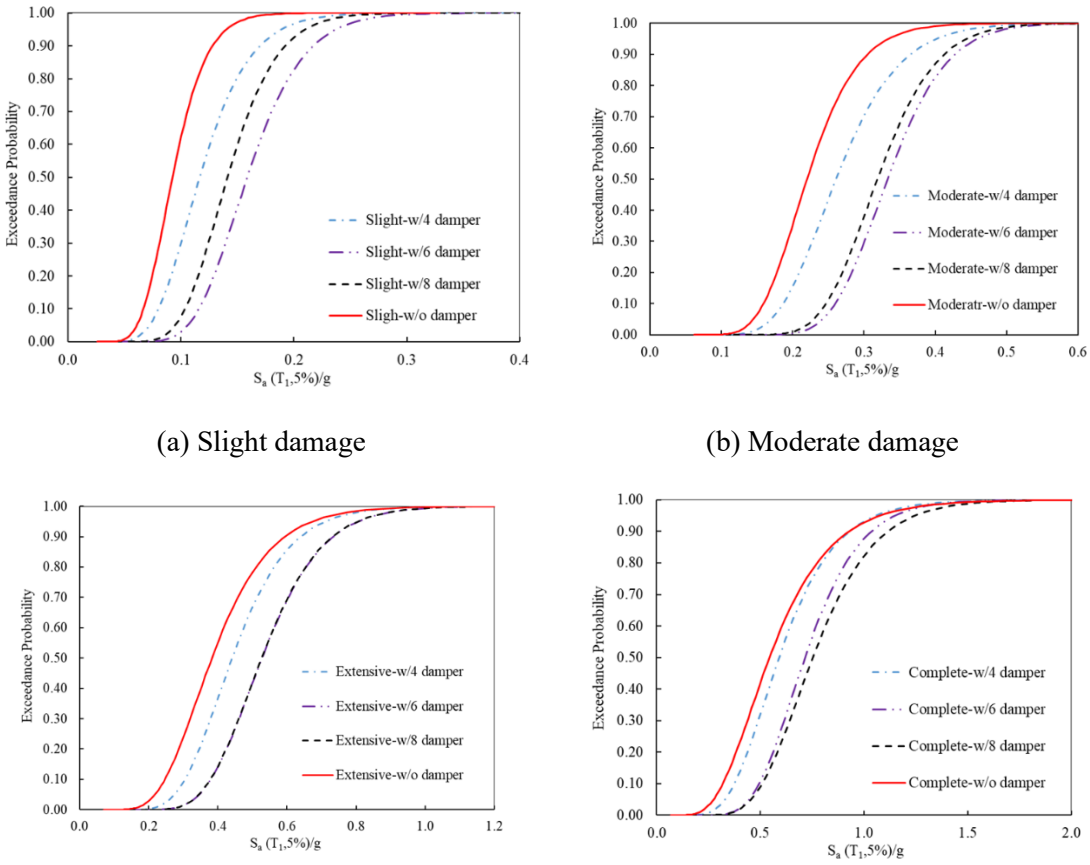

(a) Slight damage

(b) Moderate damage

(c) Extensive damage

(d) Complete damage

Figure 10. Park–Ang-based fragility curves for the 8-story RC frame at slight, moderate, extensive, and complete damage states

Table 10 presents the median spectral acceleration values corresponding to each damage state. For the six-damper configuration (which achieved the best overall performance) the median Sa increased by approximately 78%, 50%, 40%, and 33% for the Slight, Moderate, Extensive, and Complete damage states, respectively, compared with the uncontrolled frame. This demonstrates that the optimized NFVDs significantly improve the capacity of taller RC structures to withstand severe shaking before reaching critical damage levels.

Table 10: Median spectral acceleration (Sa) and improvement percentages for each damage state of the 8-story RC frame based on the Park–Ang damage index

	Sa corresponding to the mean P_f			
Condition	Slight	Moderate	Extensive	Complete
w/o damper	0.09	0.22	0.38	0.54
w/4 damper	0.11(22.2[a])	0.26(18.2)	0.44(15.8)	0.59(9.3)
w/6 damper	0.16(77.8)	0.33(50.0)	0.53(39.5)	0.72(33.3)
w/8 damper	0.14(55.5)	0.32(45.4)	0.52(36.9)	0.75(38.9)

[a] Reduction percentage with FVD compared to without FVD.

Figure 11 illustrates the difference in exceedance probability between the uncontrolled and damped configurations. The most pronounced reductions were observed in the Slight (~78%) and Moderate (~50%) states for the six-damper frame, while even at the Complete state the reduction remained around 39% for the eight-damper configuration. These results confirm that optimized viscous dampers effectively mitigate both moderate and severe damage, decreasing collapse probability and enhancing global integrity.

In summary, the fragility results for the eight-story frame follow the same general trends as the four-story model. Optimized damping systems substantially increase the median spectral acceleration associated with each damage limit, decrease response dispersion, and yield more uniform and reliable seismic behavior. These findings further validate the suitability of nonlinear viscous dampers as a cost-efficient and resilience-oriented retrofit solution for mid- to high-rise RC buildings in seismic regions.

4.4. Seismic Resilience Assessment

This section presents the resilience evaluation of both the four-story and eight-story RC frames based on the methodology described in Section 3.7. Two seismic hazard levels were considered: earthquakes with 10% and 2% probabilities of exceedance in 50 years, corresponding respectively to design-level and maximum-considered events. For each structure, the expected economic losses, functionality recovery trends, and resulting resilience indices (RI) were computed and compared between the uncontrolled and optimized configurations.

4.4.1. Four-Story Frame – Seismic Resilience Assessment

This subsection focuses on the four-story frame and investigates how the incorporation of optimized NFVDs affects structural and nonstructural losses as well as functionality recovery after an earthquake.

(a) Economic Loss Evaluation

Tables 11 and 12 summarize the expected losses for structural, acceleration-sensitive nonstructural, and drift-sensitive nonstructural components under the two hazard levels.

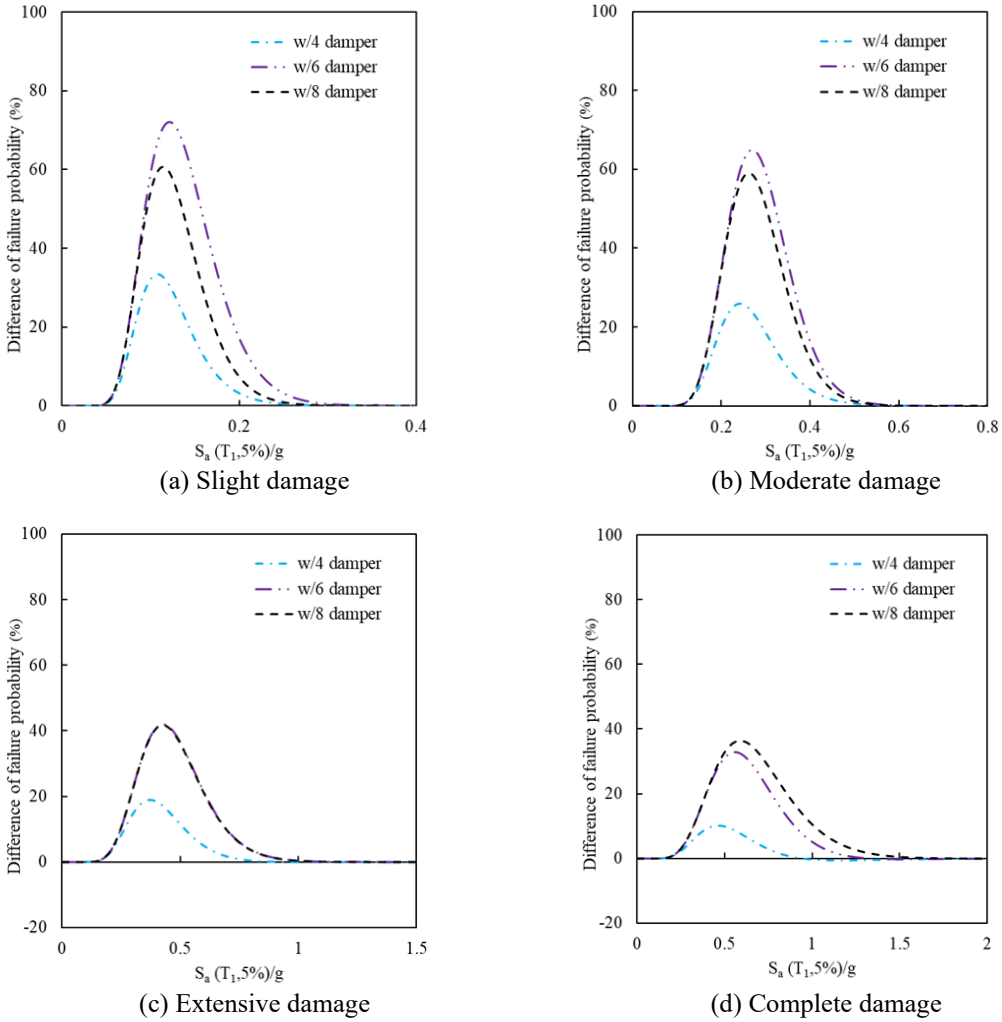

(a) Slight damage (b) Moderate damage

(c) Extensive damage (d) Complete damage

Figure 11: Difference in failure probability between uncontrolled and controlled 8-story RC frames based on the Park–Ang damage index.

Table 11: Expected structural and nonstructural loss ratios for the 4-story RC frame at a 10% probability of exceedance in 50 years

Condition	Structural Loss	Acceleration-Sensitive Non-Structural Loss	Drift-Sensitive Non-Structural Loss
w/o damper	0.1022	0.0689	0.1221
w/1 damper	0.0556(45.60[a])	0.0591(14.22)	0.1093(10.48)
w/3 damper	0.0224(70.08)	0.0349(49.35)	0.0743(39.15)
w/4 damper	0.0153(85.03)	0.0228(66.91)	0.0543(55.53)

[a] **Reduction percentage with FVD compared to without FVD.**

Table 12: Expected structural and nonstructural loss ratios for the 4-story RC frame at a 2% probability of exceedance in 50 years

Condition	Structural Loss	Acceleration-Sensitive Non-Structural Loss	Drift-Sensitive Non-Structural Loss
w/o damper	0.2662	0.2534	0.2922
w/1 damper	0.2597(2.50[a])	0.2279(10.06)	0.2737(6.33)
w/3 damper	0.1897(28.74)	0.1552(38.75)	0.2141(26.73)
w/4 damper	0.1075(59.62)	0.1122(55.72)	0.1722(41.07)

[a] **Reduction percentage with FVD compared to without FVD.**

As evident from Tables 11 and 12, the optimized nonlinear viscous dampers (NFVDs) substantially reduced all categories of loss at both hazard levels. At the 10%-in-50-years hazard level, structural losses decreased from 0.1022 in the uncontrolled frame to 0.0153 in the four-damper configuration, an 85% reduction. Similarly, acceleration- and drift-sensitive nonstructural losses were reduced by 67% and 55%, respectively. At the 2%-in-50-years level, representing more severe shaking, structural, acceleration-sensitive, and drift-sensitive nonstructural losses were reduced by approximately 60%, 56%, and 41%, respectively.

Figure 12 compares the distribution of total losses among different configurations. Structural losses dominated at higher intensities, while nonstructural losses were more pronounced during moderate events. These findings highlight the dual benefit of NFVDs in protecting both structural and functional components, thereby minimizing overall repair and downtime costs.

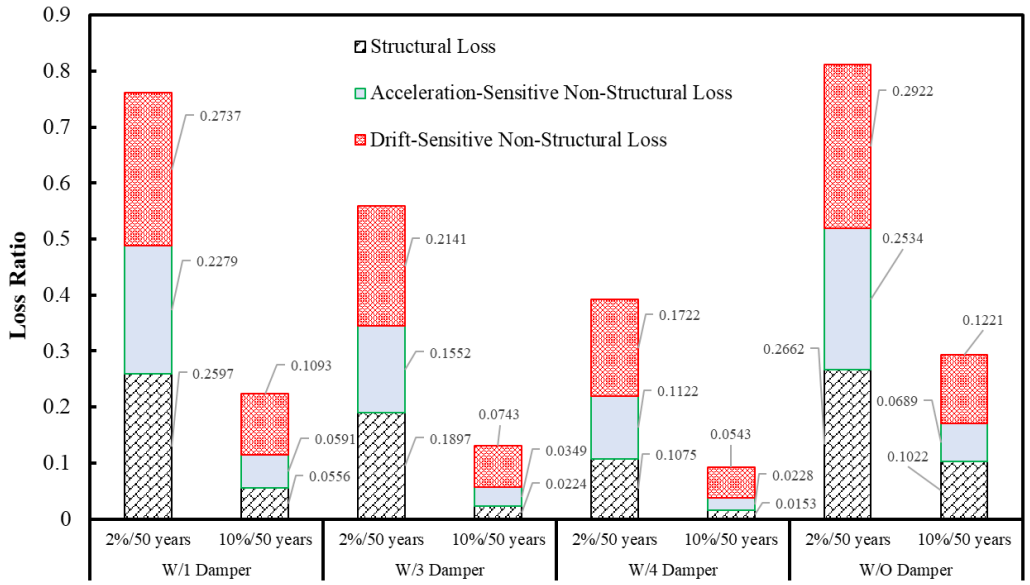

Figure 12: Comparison of total loss components for uncontrolled and controlled 4-story RC frames.

(b) Functional Recovery and Resilience Index

Figures 13 and 14 illustrate the functionality recovery curves F(t) for the four-story RC frame under the 10%- and 2%-in-50-years hazard levels. The curves represent the time-

dependent restoration of functionality, where F(t)=1.0 corresponds to full operational capacity.

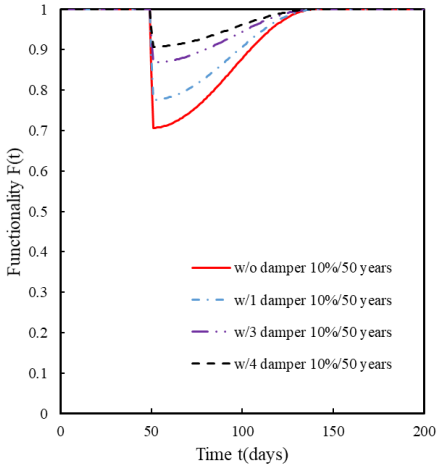

Figure 13: Functionality recovery curve F(t) for the 4-story RC frame under the 10%-in-50-years hazard level, comparing uncontrolled and controlled configurations.

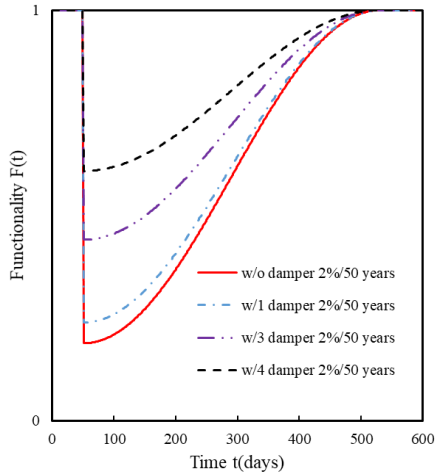

Figure 14: Functionality recovery curve F(t) for the 4-story RC frame under the 2%-in-50-years hazard level, comparing uncontrolled and controlled configurations.

The recovery duration was assumed constant for all configurations, 90 days for the 10%-in-50-years level and 480 days for the 2%-in-50-years level. Thus, improvements in resilience mainly reflect reductions in immediate functionality loss and faster recovery slopes in the controlled configurations. With NFVDs installed, the initial post-event functionality increased from about 0.68 to 0.83 at the 10% hazard level, and from 0.55 to 0.78 at the 2% level. This enhancement resulted in a 35–40% increase in the area under the recovery curve (i.e., the resilience index). Consequently, while the total recovery time remained constant, the optimized frame experienced smaller functionality drops and smoother recovery trajectories.

Table 13 presents the computed RI for all configurations. For the 10%-in-50-years event, the RI improved from 0.8534 in the uncontrolled frame to 0.9538 in the four-damper configuration (a 12% improvement).

Table 13: Seismic resilience indices (RI) and corresponding recovery times for the 4-story RC frame under 10% and 2% probabilities of exceedance in 50 years

Probability of exceedance in 50 years (%)	Recovery time (days)	Seismic resilience index			
		w/O FVD	w/1 FVD	w/3 FVD	w/4 FVD
10	90	0.8534	0.888	0.9342	0.9538
2	480	0.5941	0.6194	0.7205	0.8041

For the 2%-in-50-years event, the RI increased from 0.5941 to 0.8041, corresponding to an approximately 35% enhancement in post-earthquake functionality. These results confirm that optimized NFVDs not only reduce physical damage and economic losses but also significantly accelerate functional recovery, resulting in higher resilience against major seismic events.

4.4.2. Eight-Story Frame – Seismic Resilience Assessment

This subsection evaluates the seismic resilience of the eight-story RC frame and explores how damper distribution and building height influence recovery efficiency and loss reduction.

(a) Economic Loss Evaluation

Tables 14 and 15 present the expected structural, acceleration-sensitive, and drift-sensitive nonstructural losses for the uncontrolled and controlled configurations.

Table 14: Expected structural and nonstructural loss ratios for the 8-story RC frame at a 10% probability of exceedance in 50 years

Condition	Structural Loss	Acceleration-Sensitive Non-Structural Loss	Drift-Sensitive Non-Structural Loss
w/o damper	0.1241	0.0302	0.0939
w/4 damper	0.0905(27.07[a])	0.0217(28.14)	0.0753(19.81)
w/6 damper	0.0398(67.93)	0.0139(53.97)	0.0559(40.47)
w/8 damper	0.0480(61.32)	0.0165(45.36)	0.0627(33.23)

[a] Reduction percentage with FVD compared to without FVD.

Table 15: Expected structural and nonstructural loss ratios for the 8-story RC frame at a 2% probability of exceedance in 50 years

Condition	Structural Loss	Acceleration-Sensitive Non-Structural Loss	Drift-Sensitive Non-Structural Loss
w/o damper	0.2743	0.1396	0.2432
w/4 damper	0.2816(-2.66[a])	0.1087(22.13)	0.2108(13.32)
w/6 damper	0.2085(23.99)	0.0775(44.48)	0.1721(29.23)
w/8 damper	0.2037(25.74)	0.0882(36.82)	0.1862(23.44)

[a] Reduction percentage with FVD compared to without FVD.

The inclusion of optimized NFVDs substantially reduced total losses under both hazard levels. At the 10%-in-50-years level, the total loss decreased from 0.2482 (uncontrolled) to 0.1096 (six-damper configuration), a reduction of about 56%. At the 2%-in-50-years level, the total loss decreased from 0.6571 to 0.4581, representing a 30% overall reduction.

Figure 15 shows the total loss ratios across configurations, revealing that the most significant reductions occurred in the lower and mid-height stories, where dampers were most effective in dissipating input energy and controlling interstory drifts. These results confirm that the optimized dampers efficiently mitigate repair demands for both structural and nonstructural elements.

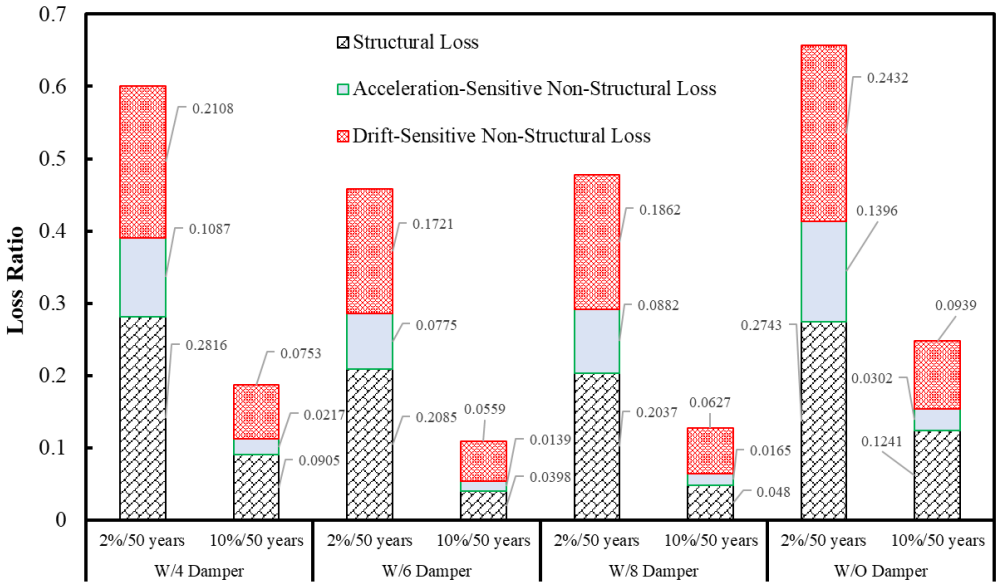

Figure 15: Comparison of total loss components for uncontrolled and controlled 8-story RC frames.

(b) Functional Recovery and Resilience Index

Figures 16 and 17 display the functionality recovery curves for the eight-story frame under the two hazard levels. The optimized configurations show a clear improvement in post-earthquake functionality compared with the uncontrolled case. At the 10%-in-50-years level, the minimum functionality increased from 0.72 to 0.88 in the eight-damper layout, while at the 2%-in-50-years level it rose from 0.50 to 0.80. These improvements correspond to an increase of approximately 38–42% in the area under the recovery curve, indicating a significant enhancement of the resilience index.

The computed resilience indices are summarized in Table 16.

For the moderate hazard level (10%-in-50-years), RI increased from 0.8759 in the uncontrolled frame to 0.9452 in the six-damper configuration (about 8% improvement). For the higher hazard level (2%-in-50-years), RI rose from 0.6714 to 0.771, marking a 15% gain in functional resilience.

In addition to these quantitative improvements, the optimized damper distribution reduced damage concentration in mid-height stories, promoting a more uniform recovery pattern

throughout the building height. This outcome emphasizes that strategically placed viscous dampers can greatly enhance the post-earthquake robustness of mid- to high-rise RC structures.

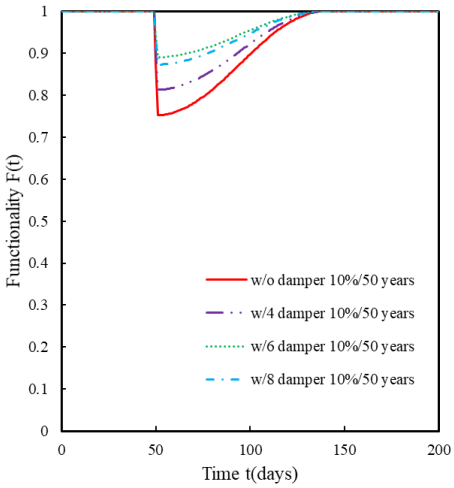

Figure 16: Functionality recovery curve F(t) for the 8-story RC frame under the 10%-in-50-years hazard level, comparing uncontrolled and controlled configurations

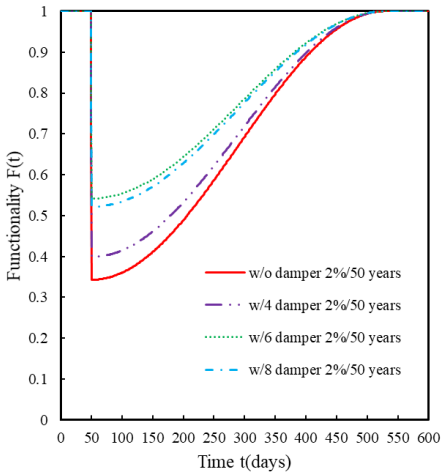

Figure 17: Functionality recovery curve F(t) for the 8-story RC frame under the 2%-in-50-years hazard level, comparing uncontrolled and controlled configurations

Table 16: Seismic resilience indices (RI) and corresponding recovery times for the 8-story RC frame under 10% and 2% probabilities of exceedance in 50 years.

Probability of exceedance in 50 years (%)	Recovery time (days)	Seismic resilience index			
		w/O FVD	w/4 FVD	w/6 FVD	w/8 FVD
10	90	0.8759	0.9063	0.9452	0.9363
2	480	0.6714	0.6995	0.771	0.761

4.5. Summary and Comparative Discussion

From a structural engineering standpoint, the comparative assessment of the four-story and eight-story RC frames offers valuable insight into the effectiveness of optimized NFVDs for improving seismic resilience. Beyond merely reducing seismic demands, the inclusion of dampers fundamentally enhanced the structural system's ability to absorb, dissipate, and recover from earthquake-induced damage. For both structures, the results of the Park–Ang damage index and fragility analyses demonstrated that the optimized dampers not only lowered global and story-level damage indices but also promoted a more uniform distribution of inelastic deformation along the building height. This uniformity is particularly important from a design perspective because it minimizes the likelihood of soft-story mechanisms, one of the most common precursors to partial collapse in conventional RC frames. The fragility curves further highlighted these improvements. The median spectral acceleration associated with each damage state increased significantly in both buildings, with more pronounced gains in the eight-story frame. This behavior can be attributed to the higher cumulative energy dissipation capacity achieved through optimized damper placement in the lower and middle stories. From a practical standpoint, these results imply that optimized viscous damping can effectively shift the performance point to higher intensity levels, thereby increasing both safety margins and serviceability under strong ground motions.

The resilience assessment provided an additional layer of understanding. For the four-story frame, the inclusion of dampers improved the resilience index by approximately 35%, while for the eight-story frame the improvement reached around 15% despite its greater complexity and higher mode effects. These increases in RI are not merely numerical, they represent substantial reductions in downtime and repair costs. In practical terms, a building equipped with optimized NFVDs could be reoccupied weeks or even months earlier after a major earthquake compared with a conventional structure.

From a retrofit design perspective, several key implications can be drawn:

1. Optimal damper placement in the lower and mid-height stories yields the greatest benefit in energy dissipation and resilience improvement.

2. Adding more dampers beyond the optimized configuration provides diminishing returns, confirming that performance efficiency is governed by optimization rather than maximization.

3. Uniformity in story-wise damage indices validates the role of NFVDs as an effective supplemental damping system for achieving performance-based and resilience-oriented design objectives in RC buildings.

Overall, the findings confirm that properly optimized nonlinear viscous dampers can transform RC moment-resisting frames from damage-prone systems into controlled and recoverable structures. In practical engineering terms, such systems deliver enhanced life safety, reduced repair costs, and accelerated functionality recovery, core principles of resilient and sustainable seismic design.

5. CONCLUSION

This study investigated the seismic performance and resilience enhancement of RC moment-resisting frames retrofitted with optimized nonlinear fluid viscous dampers (NFVDs). Two prototype buildings (a four-story and an eight-story RC frame) were analyzed to evaluate the influence of damper configuration and optimization on structural damage, fragility, and post-earthquake resilience. The key conclusions drawn from this research are summarized as follows:

Optimization Efficiency: The proposed cost-based optimization framework effectively determined the optimal number, location, and mechanical parameters of NFVDs. In both case studies, the dampers were primarily concentrated in the lower and middle stories, where interstory drifts and energy demands were the greatest. This arrangement achieved significant reductions in retrofit cost (up to 25–30%) while maintaining the desired performance objectives.

Damage Reduction and Uniformity: The inclusion of optimized NFVDs markedly reduced both global and story-level Park–Ang damage indices, shifting the overall damage condition from irreparable to repairable. For the four-story frame, the maximum story DI decreased by about 37%, while the distribution of inelastic demands along the height became substantially more uniform, eliminating potential soft-story mechanisms.

Improved Fragility Characteristics: Both drift-based and Park–Ang–based fragility analyses revealed a significant rightward shift in the fragility curves for all damage states. The increase in median spectral acceleration (Sa) reached up to 60% for the four-story and nearly 78% for the eight-story frame, confirming that optimized damping raises the intensity threshold for the onset of damage and collapse.

The inclusion of NFVDs also improved the resilience index (RI), reflecting faster recovery and reduced functional losses. The four-story frame exhibited up to a 35% increase in RI, while the eight-story frame achieved about 15%. These improvements translate to shorter downtime and reduced post-earthquake repair costs, which are critical for maintaining building operability after major events.

From a design perspective, the findings emphasize that optimization, rather than the mere addition of more dampers, governs performance efficiency. Installing a limited number of well-tuned NFVDs in strategic locations can deliver the same (or even greater) benefits than uniformly distributed systems. The results support the integration of NFVDs into performance-based and resilience-oriented design frameworks for RC buildings, particularly in regions of moderate to high seismic risk.

Recommendations for Future Work:

Future studies should extend the proposed framework to include life-cycle cost analyses, aftershock sequences, and aging effects on both dampers and RC components. Experimental validation of the optimization and recovery models is also encouraged to further demonstrate their applicability in real-world retrofitting practice.

REFERENCES

1. Kaveh A, Fahimi Farzam M, Hojat Jalali H. Statistical seismic performance assessment

of tuned mass damper inerter. *Struct Control Health Monit*. 2020;**27**:e2602.
2. Kaveh A, Mohammadi S, Hosseini OK, Keyhani A, Kalatjari VR. Optimum parameters of tuned mass dampers for seismic applications using charged system search. *Iran J Sci Technol Trans Civ Eng*. 2015;**39**:21.
3. Symans MD, Charney FA, Whittaker AS, Constantinou MC, Kircher CA, Johnson MW, et al. Energy dissipation systems for seismic applications: current practice and recent developments. *J Struct Eng*. 2008;**134**:3–21.
4. Hanson RD, Soong TT. Seismic design with supplemental energy dissipation devices. 2001.
5. Chan PT, Ma QTM. Optimising viscous damper placement in frame buildings with element exchange method for multiple seismic hazard levels. *J Earthq Eng*. 2023;**27**:3536–63.
6. Ijmulwar SS, Patro SK. Seismic design of reinforced concrete buildings equipped with viscous dampers using simplified performance-based approach. *Structures*. 2024;**61**:106020.
7. Mohemmi M, Mohammadi Dehcheshmeh E, Broujerdian V. Seismic vibration control of moment-resistant concrete frames using nonlinear viscous dampers. *Iran J Sci Technol Trans Civ Eng*. 2023;**47**:973–86.
8. Miao Z, Liu Y, Geng X, Lu Y. Evaluation of seismic collapse resistance of reinforced concrete frames designed with nonlinear viscous dampers. *Structures*. 2022;**40**:960–976.
9. De Domenico D, Ricciardi G. Earthquake protection of structures with nonlinear viscous dampers optimized through an energy-based stochastic approach. *Eng Struct*. 2019;**179**:523–39.
10. Kim J, Choi H, Min KW. Performance-based design of added viscous dampers using capacity spectrum method. *J Earthq Eng*. 2003;**7**:1–24.
11. Takewaki I. Optimal damper placement for minimum transfer functions. *Earthq Eng Struct Dyn*. 1997;**26**:1113–24.
12. Sebaq MS, Xiao Y, Song G. Damage indices of steel moment-resisting frames equipped with fluid viscous dampers. *J Asian Archit Build Eng*. 2023:1–20.
13. Kaveh A, Pirgholizadeh S, Khadem HO. Semi-active tuned mass damper performance with optimized fuzzy controller using CSS algorithm. 2015.
14. Rajana K, Wang Z, Giaralis A. Optimal design and assessment of tuned mass damper inerter with nonlinear viscous damper in seismically excited multi-storey buildings. *Bull Earthq Eng*. 2023;**21**:1509–39.
15. Hu S, Qiu C, Zhu S. Floor acceleration control of self-centering braced frames using viscous dampers. *J Build Eng*. 2023;**74**:105944.
16. Huang X. Evaluation of genetic algorithms for the optimum distribution of viscous dampers in steel frames under strong earthquakes. *Earthq Struct*. 2018;**14**:215–27.
17. Omidian P, Khaji N. A multi-objective optimization framework for seismic resilience enhancement of typical existing RC buildings. *J Build Eng*. 2022;**52**:104361.
18. Chan PT, Ma QTM. Optimising viscous damper placement in frame buildings with element exchange method for multiple seismic hazard levels. *J Earthq Eng*. 2023;**27**:3536–63.
19. Arjmand M, Naderpour H, Kheyroddin A. Optimal control based on damage of concrete moment-resisting frames retrofitted with nonlinear viscous dampers. *Structures*.

2024;**63**:106387.
20. Zhou Y, Sebaq MS, Xiao Y. Energy dissipation demand and distribution for multi-story buildings with fluid viscous dampers. *Eng Struct*. 2022;**253**:113813.
21. Park YJ, Ang AHS. Mechanistic seismic damage model for reinforced concrete. *J Struct Eng*. 1985;**111**:722–39.
22. Ostadhosein H, Hanteh M, Omidi Ashtiani Nejad M. Comparison of damage indexes in performance assessment of special concrete moment resisting frames. *J Struct Constr Eng*. 2021;**7**:244–64.
23. Haselton CB, Deierlein GG. Assessing seismic collapse safety of modern reinforced concrete moment-frame buildings. 2007;**67**.
24. Cimellaro GP, Reinhorn AM, Bruneau M. Framework for analytical quantification of disaster resilience. *Eng Struct*. 2010;**32**:3639–49.
25. Samadian D, Ghafory-Ashtiany M, Naderpour H, Eghbali M. Seismic resilience evaluation based on vulnerability curves for existing and retrofitted typical RC school buildings. *Soil Dyn Earthq Eng*. 2019;**127**:105844.
26. Mokhtari M, Naderpour H. Seismic vulnerability assessment of reinforced concrete buildings having nonlinear fluid viscous dampers. *Bull Earthq Eng*. 2022;**20**:7675–704.
27. Ashrafifar J, Estekanchi H. Life-cycle seismic fragility and resilience assessment of aging bridges using the endurance time method. *Soil Dyn Earthq Eng*. 2023;**164**:107524.
28. Huang L, Zhou Z, Wei Y, Xie Q, Sun X. Seismic performance and resilience assessment of friction damped self-centering prestressed concrete frames. *Eng Struct*. 2022;**263**:114346.
29. Forcellini D. An expeditious framework for assessing the seismic resilience (SR) of structural configurations. *Structures*. 2023;**56**:105015.
30. Zhao H, Takahashi N. Resilience evaluation of post-earthquake functional recovery for precast prestressed concrete buildings. *Appl Sci*. 2025.
31. Omidian P, Khaji N. A multi-objective optimization framework for seismic resilience enhancement of typical existing RC buildings. *J Build Eng*. 2022;**52**:104361.
32. Bakhshinezhad S, Mohebbi M. Multi-objective optimal design of semi-active fluid viscous dampers for nonlinear structures using NSGA-II. *Structures*. 2020;**24**:678–89.
33. Committee ACI. *Building Code Requirements for Structural Concrete (ACI 318-02) and Commentary (ACI 318R-02)*. American Concrete Institute; 2002.
34. American Society of Civil Engineers. *Minimum Design Loads for Buildings and Other Structures*. 2002.
35. International Code Council. *International Building Code 2003*. Illinois: International Code Council; 2004.
36. Deierlein GG, Haselton CB. Developing consensus provisions to evaluate collapse of reinforced concrete buildings. *US-Japan DaiDaiToku/NEES Workshop on Seismic Response of Reinforced Concrete Structures*. 2005:7–8.
37. Ibarra LF, Krawinkler H. Global collapse of frame structures under seismic excitations. *PEER Report 2005/06*. University of California, Berkeley, Pacific Earthquake Engineering Research Center; 2005.
38. Ibarra LF, Medina RA, Krawinkler H. Hysteretic models that incorporate strength and stiffness deterioration. *Earthq Eng Struct Dyn*. 2005;**34**:1489–511.
39. Mazzoni S, McKenna F, Scott MH, Fenves GL. *OpenSees Command Language Manual*.

Pacific Earthquake Engineering Research Center; 2006;**264**:137–58.
40. Gidaris I, Taflanidis AA. Performance assessment and optimization of fluid viscous dampers through life-cycle cost criteria and comparison to alternative design approaches. *Bull Earthq Eng*. 2015;**13**:1003–28.
41. Applied Technology Council. *Quantification of Building Seismic Performance Factors*. US Department of Homeland Security, FEMA; 2009.
42. Vamvatsikos D, Cornell CA. Incremental dynamic analysis. *Earthq Eng Struct Dyn*. 2002;**31**:491–514.
43. FEMA. *HAZUS-MH: FEMA's Methodology for Estimating Potential Losses from Disasters*. Federal Emergency Management Agency; 2004.
44. Samadian D, Ghafory-Ashtiany M, Naderpour H, Eghbali M. Seismic resilience evaluation based on vulnerability curves for existing and retrofitted typical RC school buildings. Soil Dyn Earthq Eng 2019;127:105844.
45. HAZUS M-HLEM, Methodology MLE. Earthquake Model HAZUS-MH MR5 Technical Manual. Washington, DC Fed Emerg Manag Agency 2020.